

Recent Tevatron Results on Heavy Flavours

P.H. GARBINCUS, on behalf of the CDF and D0 COLLABORATIONS

Fermi National Accelerator Laboratory, Batavia, IL 60510, USA

Summary. — CDF presents the first measurement of the B_c^\pm cross section and D0 presents the observation of a new $B_s^0\pi^\pm$ state based on the full $\sim 10 \text{ fb}^{-1}$ Run II data set at the Fermilab Tevatron 1.96 TeV $p\bar{p}$ collider.

PACS 14.40.Nd – Bottom mesons.

PACS 14.40.Rt – Exotic mesons.

PACS 12.39.Mk – Glueball and nonstandard multiquark states.

1. – Brief Descriptions of the CDF and D0 Detectors

The CDF [1] and D0 [2] detectors for Run II are illustrated below. The results presented here are based on an integrated luminosity of $\sim 10 \text{ fb}^{-1}$ for 1.96 TeV $p\bar{p}$ collisions, representing the full Tevatron Run II data sets which were taken from 2001-2011.

Both the CDF and the D0 detectors have solenoidal magnetic fields of 1.4 Tesla and 1.9 Tesla respectively, and excellent lepton coverage, detection, identification, and

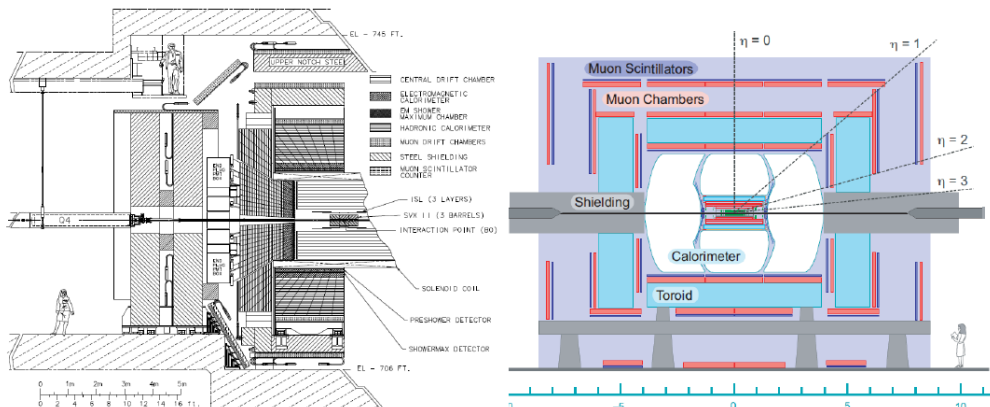


Fig. 1. – CDF (left) and D0 (right) Detectors for Tevatron Run II.

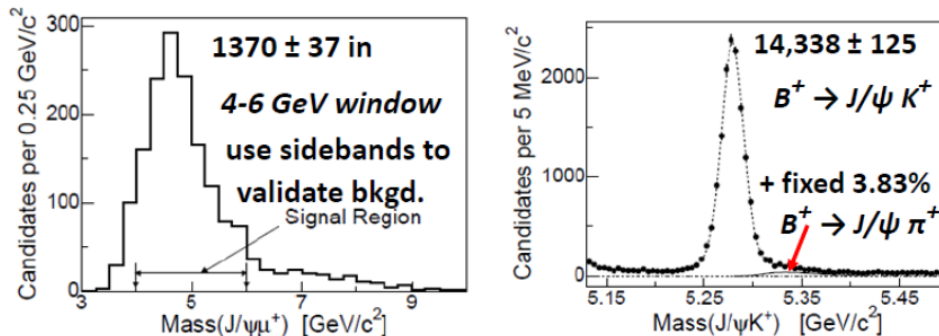


Fig. 2. – (left:) Invariant Mass($J/\psi\mu^+$) for B_c^+ candidates; (right:) Invariant Mass for $B^+ \rightarrow J/\psi K^+$ candidates with fixed 3.83% component of mis-identified $B^+ \rightarrow J/\psi\pi^+$.

triggering. Both have silicon vertex detectors to study displaced vertices from decays of particles containing b - or c -quarks. In addition, the CDF II detector features a fast displaced vertex trigger and particle identification by energy loss dE/dx in the central drift chamber and time of flight TOF . The studies presented here rely only on the muon detectors to reconstruct $J/\psi \rightarrow \mu^+\mu^-$ (not $J/\psi \rightarrow e^+e^-$). CDF detects the muons from J/ψ decay over the range $|\eta| < 1.0$ and the third muon from the B_c decay over $|\eta| < 0.6$. D0 detects muons over $|\eta| < 2$. The rapidity of a produced particle is defined as $y = 1/2 \ln((E+p_{||})/(E-p_{||}))$, where E is the energy and $p_{||}$ is the longitudinal momentum along the proton beam direction of the produced particle. The pseudorapidity is defined as $\eta = -\ln(\tan(\theta/2))$ where θ is the polar angle of the produced particles relative to the proton beam direction.

2. – CDF: Measurement of the B_c^\pm production cross section in $p\bar{p}$ collisions at $\sqrt{s} = 1.96$ TeV

The B_c^+ ($\bar{b}c$) is the most massive meson with two un-like quarks. It is only accessible at hadron colliders. CDF [3] measures the ratio

$$\mathcal{R} = \frac{\sigma(B_c^+) \mathcal{B}(B_c^+ \rightarrow J/\psi\mu^+\nu)}{\sigma(B^+) \mathcal{B}(B^+ \rightarrow J/\psi K^+)}$$

for the same kinematics of the B_c^\pm and B^+ . \mathcal{B} is the branching fractions into the observed final state. Since there is a missing neutrino in the semi-leptonic decay of the B_c^+ , the mass spectrum of $J/\psi\mu^+$ is a broad peak centered at approximately $4.65 \text{ GeV}/c^2$ as shown in Figure 2 (left). The signal region is defined as $4 < M(J/\psi\mu^+) < 6 \text{ GeV}/c^2$, and sidebands for validating the modeling of the backgrounds are defined as $3 < M(J/\psi\mu^+) < 4 \text{ GeV}/c^2$ and $6 \text{ GeV}/c^2 < M(J/\psi\mu^+)$. There are 1,370 B_c^+ candidate events within the signal mass window, 132 events in the lower sideband region, and 208 events in the upper sideband region. There are $14,338 \pm 125$ fitted number of events in the mass spectrum for the $B^+ \rightarrow J/\psi K^+$ normalization mode shown in Figure 2 (right). The spectrum also contains a fixed 3.83% component due to the reflection of $B^+ \rightarrow J/\psi\pi^+$ mis-identified as $B^+ \rightarrow J/\psi K^+$, which is also illustrated in Fig 2 (right).

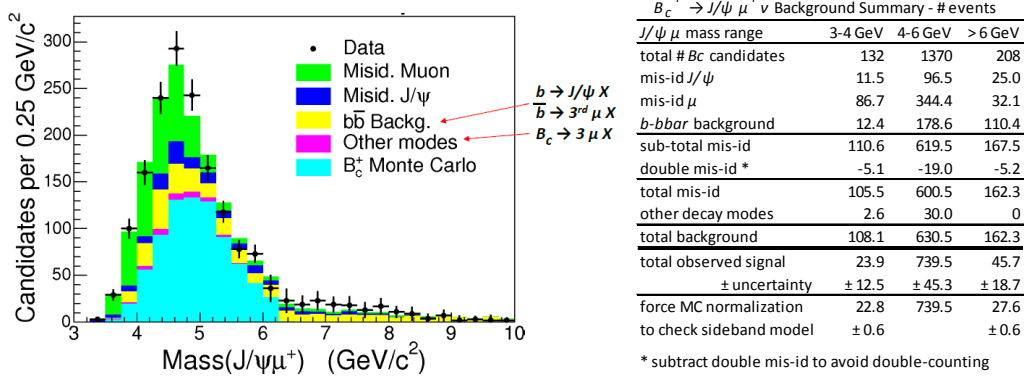


Fig. 3. – (left:) $M(J/\psi\mu^+)$ spectrum showing background components and B_c^+ candidates; (right:) Table of backgrounds and B_c^+ for signal region and sidebands.

The backgrounds under the B_c signal consist of: misidentified 3^{rd} muons; misidentified J/ψ ; correlated $b\bar{b}$ backgrounds where, for example, the $b \rightarrow J/\psi X$ and the $\bar{b} \rightarrow 3^{rd} \mu X$; and other modes where $B_c^+ \rightarrow \mu^+ \mu^- \mu^+ X$.

Figure 3 (left) shows the $M(J/\psi\mu^+)$ including these background components along with the normalized Monte Carlo simulation. Out of the $1,370 \pm 37$ B_c candidates in the signal region, 630.5 ± 20 candidates can be attributed to these backgrounds, leaving 769.5 ± 45.3 (combined statistical and systematic uncertainties) $B_c \rightarrow J/\psi\mu\nu$ events. The normalization of the Monte Carlo simulation is fixed by the total number of observed events in the signal region, then compared with the number of events observed in the upper and lower mass sideband regions, showing good agreement in the table in Figure 3 (right). The ratio \mathcal{R} can be written as

$$\mathcal{R} = \frac{N_{B_c}/\epsilon_{B_c}}{N_{B^+}/\epsilon_{B^+} \epsilon_{3^{rd}\mu}} = 0.211 \pm 0.012(\text{stat})_{-0.020}^{+0.021}(\text{syst})$$

for $p_T(B_c^+) > 6 \text{ GeV}/c$ and $|y| < 0.6$, and where the efficiencies $\epsilon(B_c^+ \rightarrow J/\psi\mu^+\nu) = (0.175 \pm 0.001)\%$ including the trigger efficiency for the 3^{rd} muon, $\epsilon(B^+ \rightarrow J/\psi K^+) = (0.688 \pm 0.002)\%$ including the trigger efficiency for the K^+ , and $\epsilon(3^{rd}\mu) = 0.962 \pm 0.007$ (stat) ± 0.021 (syst). Continuing the calculation using $\mathcal{B}(B^+ \rightarrow J/\psi K^+) = (1.027 \pm 0.031) \times 10^{-3}$ [4] and $\sigma(B^+, p_T < 6, |y| < 1) = (2.78 \pm 0.24) \mu\text{b}$ from prior CDF measurement [5] and assuming $\mathcal{R}(|y| < 1) = \mathcal{R}(|y| < 0.6)$, CDF measures $\sigma(B^+, p_T > 6, |y| < 1) \mathcal{B}(B^+ \rightarrow J/\psi K^+) = (0.602 \pm 0.034$ (stat) $_{-0.063}^{+0.060}$ (syst) ± 0.055 (other)) nb . Combining statistical and systematic uncertainties $\sigma(B_c^+) \mathcal{B}(B_c^+ \rightarrow J/\psi\mu^+\nu) = (0.60 \pm 0.09) nb$. The range of theoretical predictions [6] for the Branching Fraction $\mathcal{B}(B_c^+ \rightarrow J/\psi\mu^+\nu) = (1.15\text{-}2.37) \%$ gives $\sigma(B^+, p_T > 6, |y| < 1) \approx (25 \pm 4 \text{ to } 52 \pm 8) nb$.

3. – D0: Observation of a new $B_s^0\pi^\pm$ state

D0 [7] observes a previously unobserved structure in the mass spectrum of $B_s^0\pi^\pm$ where $B_s^0 \rightarrow J/\psi\phi$ and $J/\psi \rightarrow \mu^+\mu^-$ and $\phi \rightarrow K^+K^-$.

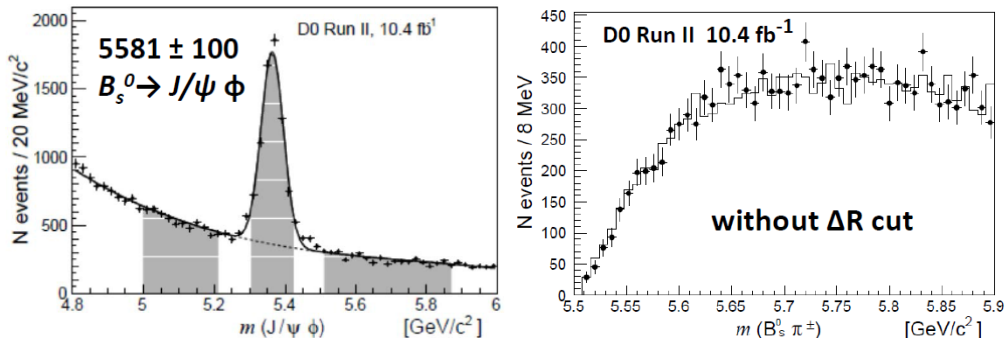


Fig. 4. – (left:) $M(J/\psi\phi)$ spectrum showing signal and sideband regions; (right:) Comparison of $M(B_s\pi)$ background spectrum without ΔR cut, points are from sidebands (area below curve in signal region) plus random pion from same primary vertex, histogram is from Monte Carlo simulation of "genuine" B_s plus random pion, with common normalization.

The selection cuts for the B_s required $p_T(K^\pm) > 0.7 \text{ GeV}/c$, and the significance of the transverse separation of the B_s decay vertex relative to the primary $p\bar{p}$ interaction vertex of $L_{xy}/\sigma_{L_{xy}} > 3$. This produced the $J/\psi\phi$ invariant mass plot in Figure 4 (left), which, when fitted, produced a sample of 5582 ± 100 B_s events plus a continuum polynomial background. The shaded regions were selection for the signal and sideband samples. The signal region within $\pm 2\sigma$ of the B_s mass peak consists of two components: a combinatorial background component (below the polynomial background curve), which is modeled by the sidebands in the data, and the genuine B_s peak (above the polynomial background curve), modeled by Monte Carlo simulation. The relative fractions of combinatorial B_s events to genuine B_s are 29% and 71%, respectively.

A single pion (either π^+ or π^-) was added to the B_s candidates in the shaded region of Figure 4 (left). The selection criteria for this π^\pm included $p_T(\pi) > 0.5 \text{ GeV}/c$; the two dimensional transverse impact parameter for the pion relative to the primary $p\bar{p}$ interaction vertex $IP_{xy} < 0.02 \text{ cm}$; and the three dimensional impact parameter, including the two transverse plus longitudinal separations, relative to the primary $p\bar{p}$ interaction vertex of $IP_{3D} < 0.12 \text{ cm}$. The $B_s\pi$ combination was required to have $p_T(B_s\pi) > 10 \text{ GeV}/c$. Finally, a "cone" cut $\Delta R = \sqrt{\Delta\eta^2 + \Delta\phi^2} = \sqrt{(\eta_{B_s} - \eta_\pi)^2 + (\phi_{B_s} - \phi_\pi)^2} < 0.3$ was applied, where ϕ is the azimuthal angle of the B_s or π . This quantity ΔR approximates the angle between the B_s and the π directions in the $p\bar{p}$ center-of-mass reference frame. The analysis was also repeated, removing and varying the ΔR cut.

The background distributions for the $B_s\pi$ mass spectra were calculated as the sum of two components: random combinatorial backgrounds for the B_s which was modeled using the data, combining a sideband $M(J/\psi\phi)$ events in Figure 4 (left) with a random π in the same data event satisfying the above selection criteria; and the random coincidence of a genuine B_s and a random π , both of which were generated by the PYTHIA Monte Carlo generator. The shape of these backgrounds are compared for no ΔR cut in Figure 4 (right), showing almost perfect agreement. These were combined in the 71%/29% ratio described above for the background shape to be used in the later fits. Figure 5 (left) shows the background shapes, both with the ΔR cut (filled points) and without the ΔR cut (open points). Both of these background shapes are fit using the form:

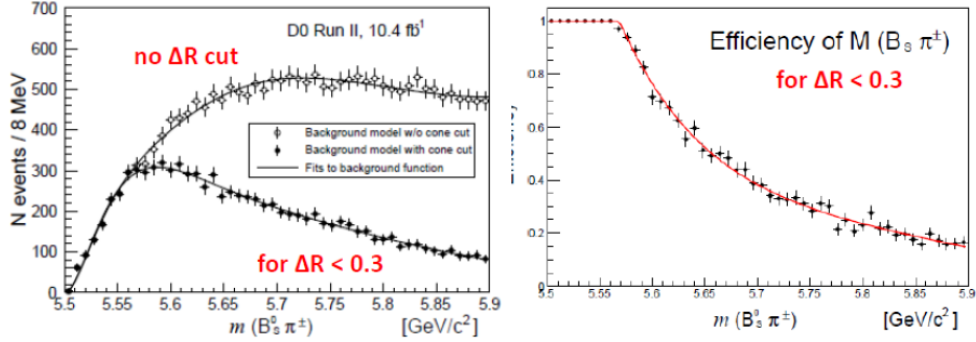


Fig. 5. – (left:) Combined $B_s\pi$ background (29% sideband + 71% "genuine B_s ") derived as illustrated in Figure 4, compared to the sideband backgrounds in the data for events with no ΔR cut and for events with $\Delta R < 0.3$; (right:) efficiency of the $\Delta R < 0.3$ cut as a function of $m_{B_s\pi}$.

$$F_{bgr}(m_{B_s\pi}) = (C_0 + C_2 \cdot m_0^2 + C_3 \cdot m_0^3 + C_4 \cdot m_0^4) \times \exp(C_5 + C_6 \cdot m_0 + C_7 \cdot m_0^2)$$

where $m_0 = m_{B_s\pi} - m_{B_s} - m_\pi$.

The observed mass spectrum for $B_s\pi$ for the $\Delta R < 0.3$ cut is shown in Figure 6 (left). The fit consists of a fixed shape (but variable normalization) for the background, from Figure 5 (left), plus an S-wave relativistic Breit-Wigner resonance, with variable width, convoluted with the Monte Carlo calculated mass resolution of $\sigma = 3.9 \text{ MeV}/c^2$. The resonance mass M_X , natural width Γ_X , and the normalization N_X (number of events) of the resonance, along with the normalization for the background were varied in the fit. This fit ($\chi^2 = 32$ for 46 degrees of freedom) determined the parameters $M_X = 5567.8 \pm 2.9$ (stat) $_{-1.9}^{+5.0}$ (syst) MeV/c^2 , $\Gamma_X = 21.9 \pm 6.4$ (stat) $_{-2.5}^{+5.0}$ (syst) MeV/c^2 , and $N_X = 133 \pm 100$ events.

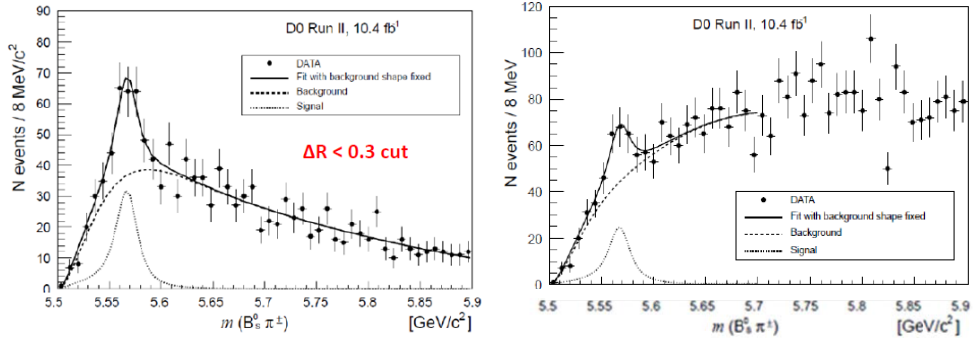


Fig. 6. – (left:) $M(B_s\pi)$ spectrum for $\Delta R < 0.3$ cut, illustrating fitted background and S-wave relativistic Breit-Wigner signal; (right:) $M(B_s\pi)$ spectrum without the ΔR cut, illustrating fitted normalizations of background and S-wave relativistic Breit-Wigner signal (fixed M_X and Γ_X , truncating fit at 5.7 GeV).

TABLE I. – *Systematic uncertainties for the observed $X(5568)$ state mass, natural width and number of events.*

Source	mass, MeV/ c^2	width, MeV/ c^2	rate, %
<i>Background shape</i>			
MC samples with soft or hard B_s^0	+0.2 ; -0.6	+2.6 ; -0.0	+8.2 ; -0.0
Sideband mass ranges	+0.2 ; -0.1	+0.7 ; -1.7	+1.6 ; -9.3
Sideband mass calculation method	+0.1 ; -0.0	+0.0 ; -0.4	+0.0 ; -1.3
MC to sideband events ratio	+0.1 ; -0.1	+0.5 ; -0.6	+2.8 ; -3.1
Background function used	+0.5 ; -0.5	+0.1 ; -0.0	+0.2 ; -1.1
B_s^0 mass scale, MC and data	+0.1 ; -0.1	+0.7 ; -0.6	+3.4 ; -3.6
<i>Signal shape</i>			
Detector resolution	+0.1 ; -0.1	+1.5 ; -1.5	+2.1 ; -1.7
Non-relativistic BW	+0.0 ; -1.1	+0.3 ; -0.0	+3.1 ; -0.9
P -wave BW	+0.0 ; -0.6	+3.1 ; -0.0	+3.8 ; -0.0
<i>Other</i>			
Binning	+0.6 ; -1.1	+2.3 ; -0.0	+3.5 ; -3.3
Total	+0.9 ; -1.9	+5.0 ; -2.5	+11.4 ; -11.2

The local significance of this signal, using the likelihood ratio, $\sqrt{-2 \ln(L_0/L_{max})} = \sqrt{43.56}$ corresponds to 6.6σ . Applying the Gross and Vitells [8] prescription for the Look Elsewhere Effect (LEE), over the range $M_{threshold}(B_s\pi) \leq M(B_s\pi) \leq M_{threshold}(B^\pm K^\mp)$, the global significance of this signal corresponds to 6.1σ .

The systematic uncertainties were studied and illustrated in Table I.

Applying the $\pm 11.3\%$ systematic uncertainty to N_X , the yield of $X(5568)$, the significance is reduced to 5.1σ including both LEE and the systematic uncertainties in the yield.

Figure 6 (right) shows the $M(B_s\pi)$ data without the ΔR cut and the fit, using the fixed background shape, and the Breit-Wigner with M_X and Γ_X fixed to the values found for the $\Delta R < 0.3$ fit of Figure 6 (left), allowing the normalizations for the background and resonance to vary. Due to not-well-modeled background for $M(B_s\pi) > 5.7 \text{ GeV}/c^2$, the fit was terminated at that point, giving $\chi^2 = 18$ for 23 degrees of freedom, and $N_X = 106 \pm 25$ events. Even without the ΔR cut, a peak in the $B_s\pi$ mass spectrum is observed with a local significance of 4.8σ .

Figure 7 shows that the fitted value of M_X is independent of the ΔR cut, demonstrating that the existence of the X particle and the position of its mass peak are not generated by the application of this cone cut.

The production rate of this new $X(5568)$ state can be estimated by $Ratio = \sigma(X) \times \mathcal{B}(X \rightarrow B_s\pi) / \sigma(B_s)$. Since we use the same B_s decay modes for the numerator and denominator of this ratio

$$Ratio = \frac{\sigma(X) \times \mathcal{B}(X \rightarrow B_s\pi)}{\sigma(B_s)} = \frac{N(X \rightarrow B_s\pi)}{N(B_s)} \frac{1}{\epsilon(\pi)}$$

where $\epsilon(\pi)$, the average efficiency of this pion over the range $10 < p_T(B_s) < 30 \text{ GeV}/c$, is 34%, giving $\sigma(X) \times \mathcal{B}(X \rightarrow B_s\pi) / \sigma(B_s) = (8.6 \pm 1.9 \text{ (stat)} \pm 1.4 \text{ (syst)}) \%$.

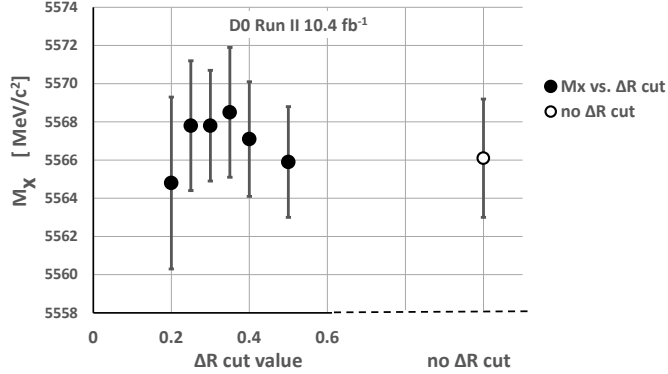


Fig. 7. – Fitted M_X vs. ΔR cut.

4. – Interpretation

We assume that X is the ground state with orbital angular momentum $L = 0$. If this state has the direct decay $X(5568) \rightarrow B_s^0 \pi^\pm$, then its spin-parity would be $J^P = 0^+$ and would be a counterpart of the $a_0^\pm(980)$ meson, replacing the $s\bar{s}$ quark components by $b\bar{s}$. If this state is really the result of the decay via $X(5568) \rightarrow B_s^{0*} \pi^\pm$ where the $B_s^{0*} \rightarrow B_s^0 \gamma$, where the γ is undetected, then the parent mass would be shifted upward by $\sim 49 \text{ MeV}/c^2$ to $5617 \text{ MeV}/c^2$ and have spin-parity of $J^P = 1^+$ and would be the counterpart of $Z_b^+ \rightarrow \Upsilon(nS) \pi^+$ [9], replacing the $b\bar{b}$ by $b\bar{s}$.

What can this $B_s \pi$ state be? Since it has a resonance width $\Gamma_X = 22 \pm 8 \text{ MeV}$, it must be a strongly decaying state. Since $B_s^0 \pi^+$ consists of a $\bar{b} s u \bar{d}$ set of valence quarks, it is clearly an exotic state. A brief bibliography of recent tetraquark and pentaquark observations is provided in reference [7]. The $X(5568)$ state is unique in that it is the first state observed containing four different quarks, and does not decay directly into a heavy $q\bar{q}$ -onia meson. It could be one of the 4 quark (tetraquark) states speculated on by Gell-Mann [10]; a loosely-bound $B - K$ molecular state [11]; or a combination of bound di-quarks considered by Maiani, *et al.* [12]. Since the Q-value of the $X(5568)$ state is only 62 MeV above the $B_s \pi$ threshold mass, and would have 206 MeV binding energy, its interpretation as a bound $B - K$ molecule is disfavored.

Since the presentation of this D0 observation, LHCb has presented preliminary results [13] of a search for this new $B_s \pi$ state in pp collisions using the $B_s \rightarrow J/\psi \phi$ and $B_s \rightarrow D_s^- \pi^+$ decay modes. LHCb did not confirm the D0 signal, quoting an upper limit as 90% CL $(\sigma(X) \times \mathcal{B}(X \rightarrow B_s \pi)) / \sigma(B_s) < 1.6\%$ for $p_T(B_s) > 10 \text{ GeV}/c$.

D0 awaits the similar studies by CDF and the other LHC experiments.

5. – Summary and Conclusions

CDF has presented the first measurement of the cross section for B_c^+ production at $|\eta| < 0.6$ and $p_T > 6 \text{ GeV}/c$ in $p\bar{p}$ production at 1.96 TeV. D0 has presented the first evidence of an exotic state $X(5568) \rightarrow B_s \pi^\pm$ consisting of four different quarks (b, s, u, d), with $M_X = 5567.8 \pm 2.9$ (stat) $_{-1.9}^{+0.9}$ (syst) MeV/c^2 , and $\Gamma_X = 21.9 \pm 6.4$ (stat) $_{-2.5}^{+5.0}$ (syst) MeV/c^2 , with a significance of 5.1σ taking into account the Look Elsewhere Effect and the systematic uncertainties in the yield of the $X(5568)$

* * *

The CDF and D0 Collaborations thank the staffs at Fermilab and collaborating institutions, and acknowledge support of the many international funding agencies which made these experimental programs possible.

D0 also thanks E. Gross and O. Vittels for useful discussions.

REFERENCES

- [1] ACOSTA D. *et al.* (CDF COLLABORATION), *Phys. Rev. D*, **71** (2005) 032001; AALTONEN T. *et al.* (CDF COLLABORATION), Operational experience, improvements, and performance of the CDF Run II silicon vertex detector, *Nucl. Instrum. Methods A*, **729** (2013) 153 (2013); AFFOLDER T. *et al.* (CDF COLLABORATION), CDF Central Outer Tracker, *Nucl. Instrum. Methods A*, **526** (2004) 249; and ABULENCIA A. *et al.* (CDF COLLABORATION), Observation of $B_s^0 \rightarrow K^+ K^-$ and Measurements of Branching Fractions of Charmless Two-Body Decays of B^0 and B_s^0 Mesons in $p\bar{p}$ Collisions at $\sqrt{s} = 1.96$ TeV, *Phys. Rev. Lett.*, **97** (2006) 211802.
- [2] ABAZOV V.M. *et al.* (D0 COLLABORATION), The upgraded D0 detector, *Nucl. Instrum. Methods Phys. Res., Sect. A*, **565** (2005) 463; ANGSTADT R. *et al.* (D0 COLLABORATION), The layer 0 inner silicon detector of the D0 experiment, *Nucl. Instrum. Methods Phys. Res., Sect. A*, **622** (2010) 298; and ABAZOV V.M. *et al.* (D0 COLLABORATION), The muon system of the Run II D0 detector, *Nucl. Instrum. Methods Phys. Res., Sect. A*, **552** (2005) 372.
- [3] AALTONEN T. *et al.*, (CDF COLLABORATION), Measurement of the B_c^\pm production cross section in $p\bar{p}$ collisions at $\sqrt{s} = 1.96$ TeV, *Phys. Rev. D*, **93** (2016) 052001.
- [4] OLIVE K.A. *et al.*, (PARTICLE DATA GROUP), Review of Particle Physics, *Chin. Phys. C* **38**, (2014) 090001.
- [5] ABULENCIA A. *et al.* (CDF COLLABORATION), Measurement of the B^+ production cross section in $p\bar{p}$ collisions at $\sqrt{s} = 1960$ GeV, *Phys. Rev. D* **75**, (2007) 012010.
- [6] see list of theoretical references 5-6 and 37-47 in reference [3] above.
- [7] ABAZOV V.M. *et al.*, (D0 COLLABORATION), Observation of a new $B_s\pi^\pm$ state, submitted to *Phys. Rev. Lett.*, arXiv:1602.07588, (2016).
- [8] GROSS E. AND VITTELS O., Trial factors for the look elsewhere effect in high energy physics, *Eur. Phys. J., C* **70**, 525 (2010).
- [9] BONDAR A. *et al.*, (BELLE COLLABORATION), Observation of Two Charged Bottomoniumlike Resonances in $\Upsilon(5S)$ Decays, *Phys. Rev. Lett.*, **108** (2012) 122001.
- [10] GELL-MANN M., A schematic model of baryons and mesons, *Physics Letters* **8** (1964) 214.
- [11] KARLINER M., Doubly Heavy Tetraquarks and Baryons, *EPJ Web Conference* **71** (2014) 00065, arXiv 1401.4058, and references therein.
- [12] MAIANI L. *et al.*, New Look at Scalar Mesons, *Phys. Rev. Lett.* **93** (2004) 212002.
- [13] AAIJ R. *et al.*, (LHCb COLLABORATION), Search for structure in the $B_s^0\pi^\pm$ invariant mass spectrum, LHCb-CONF-2016-004 (March, 2016). This is not in arXiv.